Assessment of Snow-Cover Mapping Accuracy in a Variety of Vegetation-Cover Densities in Central Alaska

D. K. Hall,* J. L. Foster,* D. L. Verbyla,† A. G. Klein,‡ and C. S. Benson§

*F*ield and aircraft measurements were acquired in April 1995 in central Alaska to map snow cover with MODIS Airborne Simulator (MAS) data, acquired from high-altitude aircraft. The Earth Observing System (EOS) Moderate Resolution Imaging Spectroradiometer (MODIS) is a 36-channel system that will be launched on the EOS-AM-1 platform in 1999. A vegetation-density map derived from integrated reflectances (R_i), from MAS data, is compared with an independently-produced vegetation type and density map derived from Thematic Mapper (TM) and ancillary data. The maps agreed to within 13%, thus corroborating the effectiveness of using the reflectance technique for mapping vegetation density. Snow cover was mapped on a 13 April 1995 MAS image, using the original MODIS prototype algorithm and an enhanced MODIS prototype algorithm. Field measurements revealed that the area was completely snow covered. With the original algorithm, snow was mapped in 96% of the pixels having <50% vegetation-cover density according to the R_i map, while in the areas having vegetation-cover densities ≥50%, snow was mapped in only 71% of the pixels. When the enhanced MODIS snow-mapping algorithm was employed, 99% of the pixels having <50% vegetation-cover density were mapped, and 98% of the pixels with ≥50% vegetation-cover density were mapped as snow covered. These results demonstrate that the enhanced algorithm represents a significant improvement over the original MODIS prototype algorithm especially in the mapping of snow in dense vegetation. The enhanced algorithm will thus be adopted as the MODIS at-launch snow-cover algorithm. Using this simple method for estimating vegetation density from pixel reflectance, it will be possible to analyze the accuracy of the MODIS snow-cover algorithm in a range of vegetation-cover in places where information on vegetation-cover density is not available from ground measurements. ©Elsevier Science Inc., 1998

INTRODUCTION AND BACKGROUND

During April 1995, a field and aircraft experiment was conducted in the boreal forest of central Alaska in support of the Earth Observing System (EOS) Moderate Resolution Imaging Spectroradiometer (MODIS) snow-cover mapping project. MODIS is scheduled for launch on the EOS AM-1 polar-orbiting platform in 1999. The MODIS Airborne Simulator (MAS), a 50-channel spectroradiometer, was flown onboard a NASA ER-2 aircraft. Field measurements were also acquired. An objective of the mission was to determine the accuracy of mapping snow in different vegetation-cover densities, using two candidate algorithms designed to map global snow cover using MODIS data. In order to do this, adequate knowledge of the vegetation type and density in the study area must first be obtained because the amount of snow mapped in a given area from a satellite is dependent, in part, on the land-cover type and vegetation-cover density. While much information can be obtained from existing satellite-derived vegetation-cover maps (e.g., Townshend et al., 1993), more detailed vegetation and forest-cover

° Hydrological Sciences Branch, NASA/GSFC, Greenbelt, Maryland
† Forest Sciences Department, University of Alaska, Fairbanks
‡ Department of Geography, Texas A&M University, College Station, Texas
§ Geophysical Institute, University of Alaska, Fairbanks

Address correspondence to D. K. Hall, Hydrological Sciences Branch, Code 974, NASA/GSFC, Greenbelt, MD 20771. E-mail: dhall@glacier.gsfc.nasa.gov

density information is necessary to validate the snow-mapping algorithm in various regions.

Snow accumulation is complex in the boreal forest, and the snowpack melts later in the spring than in adjacent tundra or prairie areas. The boreal areas are always snow covered during the winter months, but because the canopy can obscure much of the snowpack from the view of satellite sensors, it can be difficult to make accurate estimates of snow depth or snow-cover extent. The boreal forest constitutes approximately 15% of the lands normally covered by snow in the Northern Hemisphere during the winter. Reliable measurements of the snow cover in boreal areas and in other forested areas are needed.

Mapping snow cover in forested areas remains a serious limitation to the remote sensing of snow cover. In this article, we address this problem by comparing two algorithms to map snow cover using remotely sensed data in different land covers in central Alaska with the goal of improving snow-cover retrieval in forests. We first estimate vegetation-cover density using MAS-derived reflectances (Hall et al., 1998), and then we compare an independently-produced Landsat Thematic Mapper (TM)-derived land-cover type and density map with the reflectance-derived map in order to assess the accuracy of the reflectance-derived map. The Landsat-derived vegetation type and density map is assumed to be correct and is used as the standard for comparison purposes. The accuracy of mapping snow in different surface covers, particularly in forested areas, was determined for a 13 April 1995 MAS scene at a time when nearly the entire area was snow covered.

A fully automated algorithm has been developed that will map global snow cover on a daily basis at 500-m spatial resolution using MODIS data (Hall et al., 1995; Riggs et al., 1996). Snow will be identified using a technique involving the normalized difference snow index (NDSI) and the normalized difference vegetation index (NDVI) (Klein et al., 1997; in press). At launch, there will be daily, 8-day and 500-m resolution global snow-cover products, and daily, 8-day and monthly composite climate-modeling grid (CMG) products at $1/4° \times 1/4°$ spatial resolution. MODIS snow and ice data products will be archived at and distributed by the National Snow and Ice Data Center (NSIDC) in Boulder, Colorado (Scharfen et al., 1997).

Previous work has shown that a dense forest canopy can obscure the surface from not only visible sensors, but from passive-microwave sensors as well (Foster et al., 1991; Goodison and Walker, 1994; Chang et al., in press). For example, in Howland, Maine, Foster et al. (1991) found that even when the snow depth is 50 cm or more, a dense coniferous canopy, when viewed at an angle of 50°, absorbs most of the upwelling radiation emanating from the ground at the 35-GHz frequency. For visible sensors, less snow is mapped when viewed at off-

nadir angles than when viewed at nadir. Because coniferous, deciduous, and mixed coniferous–deciduous forests are prevalent in both North America and Eurasia, some snow that is present underneath a forest canopy will not be mapped from space, especially at the off-nadir sensor view angles.

Using Landsat TM and MAS data, the original MODIS prototype snow-mapping algorithm has been shown to be very effective in mapping snow cover in alpine, tundra, and prairie landscapes. Snow cover in tundra and prairie areas can be mapped with nearly 100% accuracy (when about 50% or more of the pixel is snow covered), and snow in alpine areas can be mapped with 95% accuracy (Hall et al., 1995). However, in forested areas, some snow cover which is known to be present beneath the trees is not mapped because the trees obscure the snow from view. Thus, the original snow-cover mapping algorithm was modified (Klein et al., in press).

Moderate Resolution Imaging Spectroradiometer (MODIS). MODIS is an imaging spectroradiometer that will use a cross-track scan mirror, collecting optics, and a set of individual detector elements to provide imagery of the Earth's surface and clouds in 36 discrete spectral bands. Key land-surface objectives are to study global vegetation and land cover, global land-surface change, vegetation properties, surface albedo, surface temperature, and snow and ice cover on a daily or near-daily basis (Salomonson et al., 1992; Running et al., 1994). The spectral bands cover parts of the electromagnetic spectrum from approximately 0.4 μm to 14.0 μm. The spatial resolution of the MODIS sensor at nadir will vary with spectral band and from 250 m to 1 km.

MODIS Airborne Simulator (MAS). The MAS is a spectroradiometer designed to acquire calibrated radiances. The spectral coverage and radiometric response of an existing multichannel instrument were modified to approximate the narrow spectral bands of the MODIS for measuring scientific parameters of cloud and terrestrial surface targets (King et al., 1996). The MAS, with 50 spectral bands in the wavelength range from 0.55 μm to 14.2 μm, is flown aboard a NASA ER-2 research aircraft at an altitude of about 20 km. Data from MAS channels 1–10, in the visible, near-infrared, and short-wave-infrared parts of the spectrum, are discussed in this article (Fig. 1). The MAS operates continuously during flights of up to 6 h duration while recording data on 8-mm data tape. It views 43° on either side of nadir with an Earth swath width of 37.25 km. The 15-cm aperture spatial instantaneous field-of-view is 2.5 mrad, or 50-m spatial resolution at nadir from the nominal aircraft height. The instrument consists of an optical bench-mounted sensor within an aluminum housing, a digitizer/controller, and tape drives. The MAS has a 16-bit digitization, allowing 12 bits of noise-free data.

Description of the MODIS snow-mapping algorithms. Prototype snow-mapping algorithms have been devel-

Figure 1. Schematic showing the wavelength regions of the Moderate Resolution Imaging Spectroradiometer (MODIS), MODIS Airborne Simulator (MAS), and Landsat Thematic Mapper (TM) sensors in the visible through short-wave infrared part of the electromagnetic spectrum. The numbers refer to the band numbers of the respective sensor. The numbers on top in bold refer to the MODIS land bands.
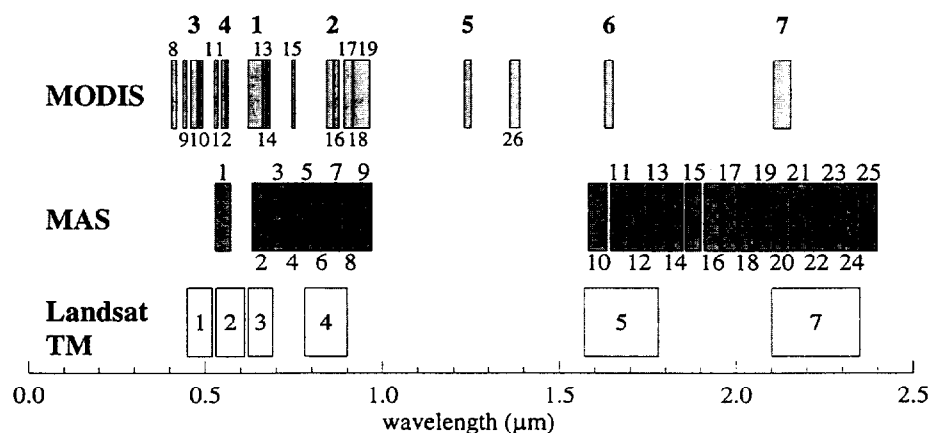
oped to map snow using TM and MAS data as surrogates for MODIS data. The heritage for the algorithms comes from earlier work (Kyle et al. 1978; Bunting and d'Entremont, 1982; Dozier, 1989) where the normalized difference of the reflectance of a visible and a short-wave-infrared band is used to identify snow. The reflectance of snow is very high in the visible part of the spectrum where TM Band 2 (0.52–0.6 μm) is located, and near zero in the short-wave infrared part of the spectrum where TM Band 5 (1.55–1.75 μm) is located. The algorithms are designed to detect snow, if present, in each pixel. Optimum detection of snow cover by reflectance properties requires that data be expressed in physical units, for example, reflectance. Thus, the MAS and TM digital number (DN) data are converted to reflectances. DNs are converted to at-satellite reflectances using recorded gains and offsets and the formulation of Markham and Barker (1986) for conversion to at-satellite reflectance. MAS reflectances are also calculated from the DNs using formulation designed specifically for the MAS (Gumley et al., 1994). Then the NDSI is calculated in Eqs. (1) and (2) using the reflectance values. For the TM data,

$$NDSI=(TM\ 2-TM\ 5)/(TM\ 2+TM\ 5). \tag{1}$$

For the MAS data,

$$NDSI=(MAS\ 2-MAS\ 10)/(MAS\ 2+MAS\ 10), \tag{2}$$

where MAS Channel 2 covers from 0.631 μm to 0.684 μm, and MAS Channel 10 covers from 1.582 μm to 1.635 μm. In the original MODIS snow-mapping algorithm, snow is mapped in a pixel when the NDSI is $\geq$0.4. In this binary classification, a pixel that is approximately 50% or more covered by snow is considered snow-covered. Since water may also have an NDSI $\geq$0.4, an additional test is necessary to separate snow and water. Snow and water may be discriminated because the reflectance of water is <11% in TM Band 4 (0.76–0.9 μm); snow is mapped when the TM Band 4 or the MAS Channel 6 (0.806–0.848 μm) reflectance is >11%, and the NDSI $\geq$0.4.

In order to improve the algorithm so that it maps more snow that is known to exist in forests, an enhancement of the original algorithm was developed. The normalized difference vegetation index (NDVI) and the NDSI are used together in order to discriminate between snow-free and snow-covered forests.

The major limitation in the original snow-mapping algorithm is that the 0.4 NDSI threshold is not well suited to the detection of snow in forests, as many snow-covered forests have an NDSI value below 0.4. However, these forests will have higher NDVI values than the surrounding, nonforested snow-covered areas. Thus by using the NDSI and NDVI in combination, it is possible to lower the NDSI threshold for forested pixels. In this manner, the snow-classification accuracy can be improved in forested areas without compromising performance in other land covers where the classification accuracy of the original algorithm is already high.

This new NDSI-NDVI field is designed to capture as much of the variation in NDSI-NDVI values observed in the snow-covered forests as possible while minimizing inclusion of non-forested pixels (Fig. 2). It was designed to include forest-covered pixels that have NDSI values lower than the current threshold, yet have NDVI values lower than would be expected for snow-free conditions (Klein et al., in press).

One additional problem occurs in detection of snow under certain forest types. Many forest types, most notably black spruce, have very low reflectances in the 1.6 μm wavelength region (TM Band 5). These low reflectances cause the denominator in the NDSI to be quite small, and only small increases in the visible wavelengths (e.g., TM Band 2) are required to make the NDSI value high enough to classify a pixel as snow. For instance, if the short-wave-infrared reflectance is 5%, then it may only take a visible reflectance of 12% for the NDSI to exceed the 0.40 threshold. This problem is exacerbated when the NDSI/NDVI threshold is employed, as lower NDSI values will be classified as snow. To limit errors of commission in the enhanced MODIS snow-cover
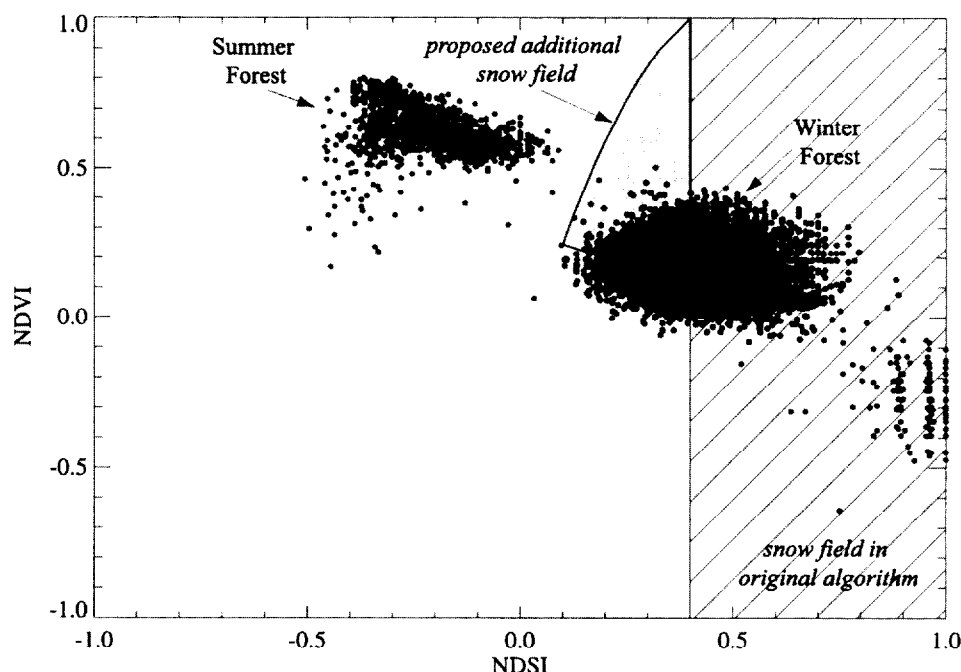
Figure 2. NDSI versus NDVI plot for coniferous and deciduous forest stands in central Saskatchewan. Gray points are from a 6 August 1990 TM scene and black points are from a 6 February 1994 TM scene. The hatched area contains NDSI values considered to be snow in the original algorithm, while the gray-shaded region represents the new field for capturing snow-covered forests in the enhanced MODIS snow-mapping algorithm (from Klein et al., in press).

mapping algorithm, a visible threshold is used to prevent pixels with very low visible reflectances from being classified as snow as has previously been suggested (Dozier, 1989). Here a threshold of 10% in TM band 2 was used. Landsat TM band 2 was selected over TM Band 1 (0.45–0.52 μm) because of the effects of Rayleigh scattering are greater at shorter wavelengths.

To map snow cover following the MODIS launch, the MODIS snow-mapping algorithm will employ at-satellite reflectances in MODIS Bands 4 (0.545–0.565 μm) and 6 (1.628–1.652 μm) to calculate the NDSI. A pixel will be mapped as snow if the NDSI is $\geq$0.4 and reflectance in MODIS Band 2 (0.841–0.876 μm) is >11%. However, if the MODIS Band 4 reflectance is <10%, then the pixel will not be mapped as snow even if the other criteria are met. This prevents pixels containing very dark targets from being mapped as snow. In addition, MODIS Bands 1 (0.620–0.670 μm) and 2 will be used to calculate the NDVI to permit mapping snow in forests. If a pixel has NDSI and NDVI values within an irregular polygon as determined from canopy-reflectance modeling (Fig. 2), it is mapped as snow covered.

RESULTS AND DISCUSSION

Vegetation-cover density map derived from MAS-derived reflectances. Vegetation-cover density was estimated

from integrated reflectance (R_i) values in the 13 April 1995 MAS scene acquired over central Alaska (Fig. 3 top) in the following manner. The integrated reflectance is the reflectance integrated over a portion of the electromagnetic spectrum (Hall et al., 1989). The highest R_i values correspond to snow-covered bare areas or areas covered with very low vegetation, snow-covered ice, or low-density broadleaf forests, and the lowest R_i values correspond to the low-, medium-, and high-density spruce and mixed forests and the medium- and high-density broadleaf forests. A linear relationship between reflectance and vegetation-cover density is developed from the maximum and minimum reflectances in the scene as has been done by other researchers (Robinson and Kukla, 1984; 1985; Foster et al., 1994) to estimate snow albedo and vegetation density. Ten categories of reflectance are delineated. To simplify the map, we divided the map into only two categories: vegetation-cover density of <50% and $\geq$50% (Fig. 3 bottom). For this study, this map was compared with a vegetation type and density map derived from TM and ancillary data (described below). Then, the original and the enhanced MODIS snow-mapping algorithms were run on the 13 April MAS scene, and the accuracy of snow mapping in different vegetation types and densities was assessed. On 13 April, the study area in central Alaska was completely snow
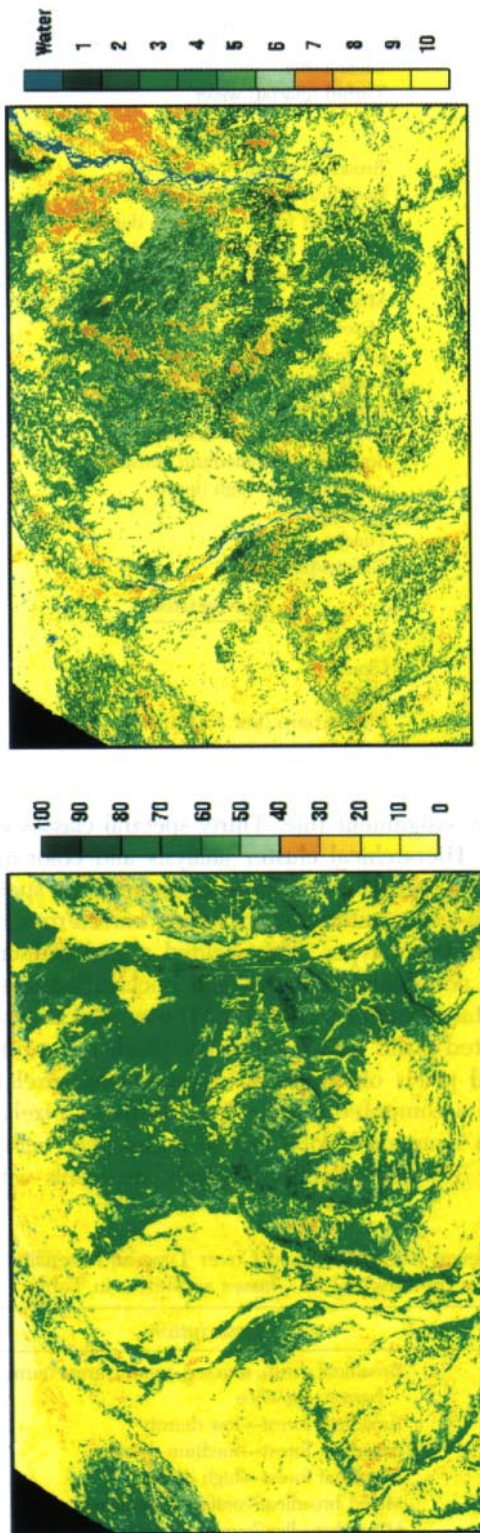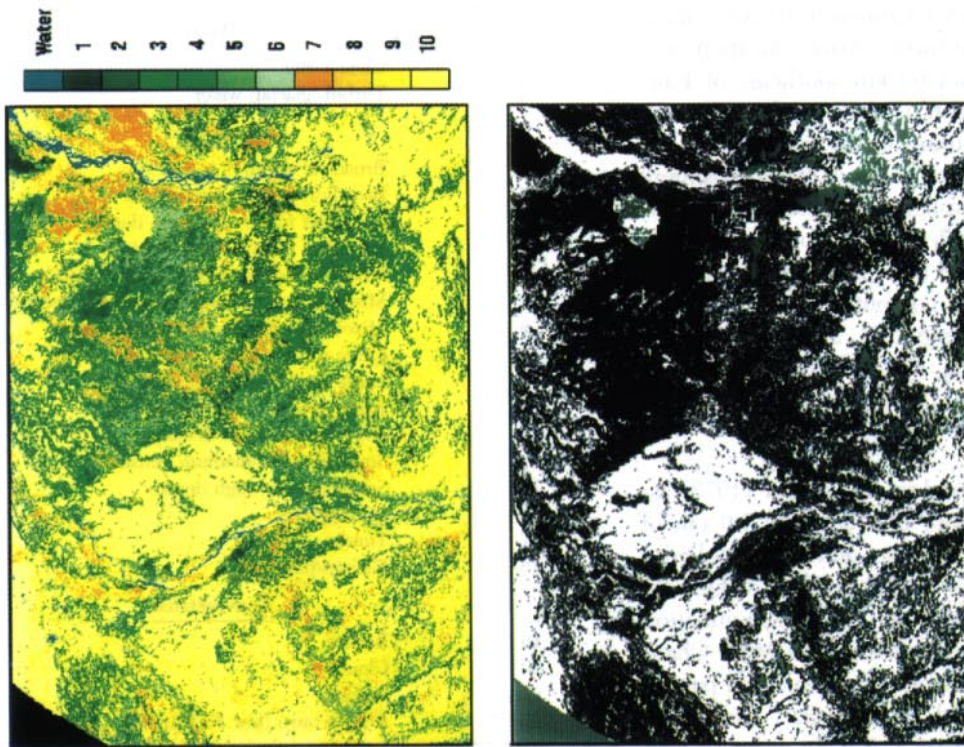
Figure 4. Vegetation type and density map determined from Landsat TM (22 June 1991) and ancillary data. 23 classes of vegetation type and density were combined to yield 11 classes as shown (top). The black and white image (bottom) shows only two categories of vegetation density. Black includes the following classes: low, medium, and high density spruce and mixed forests, and medium and high density broadleaf forests. White represents water, low-density broadleaf forests, and broadleaf shrub, muskeg, tundra, grasses, burned areas, and nonvegetated areas. Gray represents clouds, shadows, and other areas that could not be classified.

Figure 3. Vegetation-cover density map of a subscene of the 13 April 1995 MAS scene over central Alaska, derived from MAS-derived reflectance data. Vegetation-cover density is given from 0–100% in increments of 10 as shown in the various colors (top). The black and white image (bottom) shows the same area as in the color image, but only two categories of vegetation density are shown. Black represents vegetation density ≥50%, and white represents vegetation density <50% as derived by the reflectance method. Gray represents clouds, shadows, and other areas that could not be classified.

covered except for the downtown area of Fairbanks, but the snow was melting rapidly.

The maximum and minimum visible/near-infrared integrated reflectances (MAS Channels 1–9) were measured in the 13 April MAS subscene from a location near Harding Lake which is about 60 km southeast of Fairbanks. Determination of the R_i is done in the following manner. The energy distribution in the spectrum of direct solar radiation at different levels of the atmosphere is known for specified atmospheric conditions. By knowing the reflectance of a specified target (for example, the reflectance of snow, measured using the MAS sensor), at certain wavelengths, one can compute R_i for each pixel in the scene, using solar energy, SE, and measured reflectance, R, according to Eq. (3) (Hall et al., 1989):

$$R_i = \left(\sum_{0.527}^{0.970} (SE \cdot R) \right) \div \sum_{0.527}^{0.970} SE, \qquad (3)$$

where SE, in W cm^{-2}, is found in Kondrat'ev (1973) assuming a clear sky atmosphere that contains 1.0 cm of precipitable water, 0.35 cm of ozone, and an aerosol concentration of 200 cm^{-3} at the Earth's surface. Values are given for an atmospheric mass, $m = 1.5$. The summation from 0.527 μm to 0.970 μm represents the MAS Channels 1–9. Data from the visible and near-infrared part of the spectrum were also used by Robinson and Kukla (1985) and Knap and Oerlemans (1996) in order to map snow and ice albedo.

TM-derived vegetation map of central Alaska. A vegetation type and density map which shows 23 distinct land-cover types or forest-cover densities was developed using a 22 June 1991 TM scene and ancillary data. First, the original TM pixels were stratified into separate grids: snow/ice and clouds, nonvegetated pixels based on NDVI, and vegetated pixels stratified into separate grids of level, northerly and southerly slopes. For all cold pixels (when TM Band 6 (10.4–12.5 μm) DNs are <110), a TM Band 7 (2.08–2.35 μm) DN threshold was used to separate clouds from snow/ice (TM Band 7<50=snow/ice, TM band 7≥50=clouds). This yielded a grid of snow/ice, clouds, and unclassified pixels.

Vegetated versus nonvegetated pixels were then distinguished using an NDVI threshold value. The NDVI was computed in Eq. (4) from DNs and scaled from 0 to 200:

$$NDVI = int(((float(tm4\text{-}rec - tm3\text{-}rec)/float$$
$$\times (tm4 - rec + tm3 - rec)) + 1.0) \cdot 100), \qquad (4)$$

where tm4−rec and tm3−rec refer to TM digital numbers from the rectified TM Bands 4 and 3 (0.63–0.69 μm), respectively.

Then, using 1:15,840 color-infrared aerial photographs acquired in 1994, vegetated versus nonvegetated surfaces were separated by a DN threshold value of 127. For all nonvegetated pixels, an ISODATA unsupervised classification was performed using maximum likelihood

Table 1. Classes of Land Cover Type and Vegetation Density Computed Using TM and Ancillary Data

Class	Description
	Water
1	Clear water
2	Turbid (glacial) water
	Vegetated
3	Broadleaf shrub
4	Broadleaf forest—low density
5	Broadleaf forest—medium density
6	Broadleaf forest—high density
7	Mixed broadleaf/conifer—low density
8	Mixed broadleaf/conifer—medium density
9	Mixed broadleaf/conifer—high density
10	Large spruce—low density
11	Large spruce—medium density
12	Large spruce—high density
13	Small spruce—low density
14	Small spruce—medium density
15	Small spruce—high density
16	Muskeg
17	Tundra
18	Grasses/past burn
	Nonvegetated
19	Barren
20	Clouds
21	Shadow
23	Recent burn (low NDVI)

as the class assignment rule. Thirty spectral classes were generated. Hierarchical cluster analysis and color-infrared aerial photography were used to group these spectral classes into clear water, turbid water, barren/rock, and recent burn cover types. This yielded a grid containing these four nonvegetated classes and unclassified pixels.

A digital elevation model (DEM) was used to stratify the vegetated pixels into: level pixels, pixels on northerly slopes, and pixels on southerly slopes. Level pixels are pixels with a computed slope <5%. Northerly pixels are pixels with computed slope ≥5 % and aspect between 0–90° and 315–360°. Southerly pixels are pixels with a

Table 2. Eleven Classes of Land Cover Type and Density Derived from the Original 23 Classes as Shown in Table 1

Class	Description
1	Broadleaf shrub, muskeg, tundra, grass burn, barren, snow/ice
2	Broadleaf forest—low density
3	Broadleaf forest—medium density
4	Broadleaf forest—high density
5	Mixed broadleaf/conifer—low density
6	Mixed broadleaf/conifer—medium density
7	Mixed broadleaf/conifer—high density
8	Large and small spruce—low density
9	Large and small spruce—medium density
10	Large and small spruce—high density
11	Clear water and turbid (glacial) water

computed slope ≥5% and an aspect between 90° and 315°. Thus there are three grids for selecting the TM bands for classification (level pixels, northerly pixels, and southerly pixels). An ISODATA unsupervised classification was performed using maximum likelihood as the class assignment rule with target of 30 spectral classes for each of the three grids. Hierarchical cluster analysis and color-infrared aerial photography was then used to group these spectral classes. This yielded three more grids (one from each slope class, i.e., water, vegetated, and nonvegetated) of vegetation classes (Table 1).

Snow/clouds, unvegetated classes (clear water, turbid water, barren/rock, and recent burn cover) and vegetated classes were merged to create a classified image. Interactive editing was used to correct any cloud shadow that was misclassified as clear water. The 23 classes were then simplified into 11 classes (Table 2) to produce an image as shown in Figure 4 (top).

Error analysis of the TM-derived vegetation type and density map. The Landsat TM forest density classes were assessed for classification error by using the color-infrared aerial photography as the reference data. The photography covered approximately 1% of the TM scene. Thirty points were randomly generated within each forest (broadleaf, conifer, mixed) class. These points were displayed over the TM color-infrared image (TM4=red, TM3=green, TM2=blue). Each displayed point was then located on a color-infrared photograph and stereoscopically interpreted to forest type (broadleaf, conifer, mixed) and density class (<30, 30–60, and >60 crown closure). All photointerpretation was done without knowledge of the TM class of the randomly-located points. The photo-interpreted results were compared with the TM classifications. The overall accuracy was found to be 70%. This estimate of the classification accuracy assumes the reference data to be without photointerpretation errors.

Comparison of vegetation-type and density map derived from TM and ancillary data versus map derived from MAS reflectances. The R_i-derived and the TM-derived maps (Figs. 3 and 4, respectively) were produced by completely independent methods. The R_i-derived and the TM-derived maps were digitally registered and compared after removing from consideration all pixels containing clouds and cloud shadows. In the areas of the R_i density map (Fig. 3—bottom) that were classified as <50% vegetation-cover density, the following land covers (as mapped on the TM-derived vegetation type and density map) were found: barren, snow/ice, recent burn, tundra, muskeg, grasses/past burn, broadleaf shrub, and low-density broadleaf forest. These classes, grouped as one (Fig. 4—bottom), correspond to within about 13% with the <50% vegetation-density category on the R_i map. In areas classified as ≥50% vegetation-cover density on the R_i map, all medium or high density forests, and all spruce forests were found. The similarity of these independently-derived maps [Fig. 3 (bottom) and Fig. 4 (bottom)] shows that the reflectance-derived technique of es-

Table 3. Results of Snow Mapping in Each of the 23 Vegetation Type and Density Categories Derived from TM and Ancillary Data, Using the Enhanced MODIS Snow-Mapping Algorithm

	Total Pixels	Number of Pixels Mapped as Snow	% Snow Cover Mapped
1. Clear water	491	—	—
2. Turbid (glacial) water	6307	—	—
3. Broadleaf shrub	126522	125171	98.93
4. Broadleaf forest—low density	19499	19401	99.50
5. Broadleaf forest—medium density	15122	15040	99.46
6. Broadleaf forest—high density	71914	68537	95.30
7. Mixed broadleaf/conifer—low density	50833	50220	98.79
8. Mixed broadleaf/conifer—medium density	31470	30964	98.39
9. Mixed broadleaf/conifer—high density	43129	42609	98.79
10. Large spruce—low density	0357	20223	99.34
11. Large spruce—medium density	25548	25245	98.81
12. Large spruce—high density	6756	6659	98.56
13. Small spruce—low density	32345	32210	99.58
14. Small spruce—medium density	41068	40950	99.71
15. Small spruce—high density	15384	15282	99.34
16. Muskeg	82254	81913	99.59
17. Tundra	22816	22413	98.23
18. Grasses past burn	19081	18988	99.51
19. Barren	17180	16857	98.12
20. Clouds	7413	—	—
21. Shadow	18798	—	—
22. Snow/ice	3657	3563	97.43
23. Recent burn (low NDVI)	29868	29766	99.66

timating vegetation-cover density can be successfully used to estimate vegetation-cover density over large areas when the ground is completely snow covered, at least in central Alaska.

Comparison of results of the original versus the enhanced snow-mapping algorithms. Using the original MODIS snow-mapping algorithm on the 13 April 1995 MAS scene, 96% of the pixels are mapped as snow covered in the less-dense vegetation category (<50% density according to the R_i map), and 71% of the pixels are mapped as snow covered in the more-dense vegetation category (≥50%). Using the enhanced MODIS snow-mapping algorithm, 99% of the pixels are mapped as snow covered in the less-dense vegetation-cover density category derived from the R_i map, and 98% of the pixels are mapped as snow covered in the more-dense vegetation-cover density category. Using the enhanced algorithm, the land cover in which the least amount of snow is mapped is the high-density broadleaf forest (95% of the pixels), even though the leaves were not on the trees when the snow was mapped using the MAS data acquired on 13 April 1995. Even less snow was mapped there, than in the high-density large spruce (99% of the pixels) or the high-density mixed forest (99% of the pixels) (Table 3).

CONCLUSIONS

At least in central Alaska, the technique of using the wintertime reflectances as a surrogate measure of vegetation density (Robinson and Kukla, 1985; Foster et al., 1994) appears to be valid. In this article, we compared a vegetation-density map derived from integrated reflectances (from Channels 1–9 of MAS data), with an independently produced vegetation type and density map (derived from TM and ancillary data). The TM-derived map is assumed to be an accurate depiction of the actual vegetation type and density. All spruce forests, and all coniferous and deciduous medium- and high-density forests, were classified as corresponding to vegetation densities of ≥50% on the R_i map, while all other surface covers, including low-density broadleaf forests, were classified as corresponding to vegetation densities of <50%. The maps agreed to within 13%. The forest-cover type and density must be considered when determining the accuracy of snow mapping in different land covers. As determined from 11 land-cover categories from the TM-derived map, the least amount of snow (95%) was mapped in the high-density broadleaf forests using the enhanced algorithm.

Snow on the 13 April 1995 MAS scene was mapped using the original MODIS prototype algorithm and the enhanced prototype algorithm. Field measurements revealed that the area was completely snow-covered. With the original algorithm, 96% of the pixels were snow-covered in the areas having <50% vegetation-cover density,

while, in the areas having vegetation-cover densities ≥50%, only 71% of the pixels were mapped as snow-covered. When the enhanced MODIS snow-mapping algorithm was employed, 99% of the pixels were mapped as snow in the less-dense vegetation (<50% density) category, and 98% of the snow pixels were mapped as snow in the denser vegetation category (≥50% density). The enhanced algorithm represents a significant improvement over the original MODIS prototype algorithm in mapping snow in dense forests and it will thus be adopted as the MODIS at-launch snow-cover mapping algorithm.

REFERENCES

Bunting, J. T., and d'Entremont, R.P. (1982), Improved cloud detection utilizing defense meteorological satellite program near infrared measurements, AFGL-TR-82-0027, Environmental Research Papers No. 765, Air Force Geophysics Laboratory, Hanscom AFB, MA, 91 pp.

Chang, A. T. C., Foster, J. L., Hall, D. K., et al. (in press), Snow parameters derived from microwave measurements during the BOREAS winter field campaign. *J. Geophys. Res.* 102(D24):29,663–29,671.

Dozier, J. (1989), Spectral signature of alpine snow cover from the Landsat thematic mapper. *Remote Sens. Environ.* 28: 9–22.

Foster, J. L., Chang, A. T. C., Hall, D. K., and Rango, A. (1991), Derivation of snow water equivalent in boreal forests using microwave radiometry. *Arctic* 44(Suppl.1):147–152.

Foster, J. L., Chang, A. T. C., and Hall, D. K. (1994), Snow mass in boreal forests derived from a modified passive microwave algorithm. In *Multispectral and Microwave Sensing of Forestry, Hydrology, and Natural Resources* (E. Mougin, K. J. Ranson, and J. A. Smith, Ed.), 26–30 September, Rome, Italy, pp. 605–617.

Goodison, B. E., and Walker, A. E. (1994), Canadian development and use of snow cover information from passive microwave satellite data. In *Passive Microwave Remote Sensing of Land-Atmosphere Interactions*, ESA/NASA International Workshop (B. J. Choudhury, Y. H. Kerr, E. G. Njoku, and P. Pampaloni, Eds.), pp. 245–262.

Gumley, L., Hubanks, P., and Masuoka, E. (1994), *MODIS Airborne Simulator Level 1B Data User's Guide*, http://ltpsun.gsfc.nasa.gov/MAS/Home.html.

Hall, D. K., Chang, A. T. C., Foster, J. L., Benson, C. S., and Kovalick, W. M. (1989), Comparison of in situ and Landsat derived reflectance of Alaska glaciers. *Remote Sens. Environ.* 28:23–31.

Hall, D. K., Riggs, G. A., and Salomonson, V. V. (1995), Development of methods for mapping global snow cover using Moderate Resolution Imaging Spectroradiometer (MODIS) data. *Remote Sens. Environ.* 54:127–140.

Hall, D. K., Foster, J. L., Chang, A. T. C., Benson, C. S., and Chien, J. Y. L. (1998), Determination of snow-covered area in different land covers in central Alaska from aircraft data—April 1995. *Ann. Glaciol.* 26:149–155.

King, M. D., Menzel, W. P., et al. (1996), Airborne scanning spectrometer for remote sensing of cloud, aerosol, water vapor, and surface properties. *J. Atmos. Ocean. Technol.* 13(4):777–794.

Klein, A. G., Hall, D. K., and Riggs, G. A. (1997), Improving the MODIS global snow-mapping algorithm. In *International Geoscience and Remote Sensing Symposium 1997, IGARSS '97*, Proceedings of the 3–8 August 1997 Meeting, Singapore, pp. 619–621.

Klein, A. G., Hall, D. K., and Riggs, G. A. (in press), Improving snow-cover mapping in forests through the use of a canopy reflectance model. *Hydrol. Process.*

Knap, W. H., and Oerlemans, J. (1996), The surface albedo of the Greenland ice sheet: satellite-derived and in situ measurements in the Sondre Stromfjord area during the 1991 melt season. *J. Glaciol.* 42(141):364–374.

Kondrat'ev, K. Ya., Ed. (1973), *Radiation Characteristics of the Atmosphere and the Earth's Surface*, NASA, Washington, DC, 580 pp.

Kyle, H. L., Curran, R. J., Barnes, W. L., and Escoe, D. (1978), A cloud physics radiometer. In *Third Conference on Atmospheric Radiation*, Davis, CA, pp.107—109.

Markham, B., and Barker, J. L. (1986), Landsat MSS and TM post-calibration dynamic ranges, exoatmospheric reflectances and at-satellite temperatures. *EOSAT Tech. Notes* 1(Aug.):3–8.

Riggs, G. A., Hall, D. K., and Salomonson, V. V. (1996), Recent progress in development of the Moderate Resolution Imaging Spectroradiometer snow cover algorithm and product. In *Proceedings of IGARSS'96*, Lincoln, NE, pp.139–141.

Robinson, D. A., and Kukla, G. (1984), Albedo of a dissipating snow cover. *J. Clim. Appl. Meteorol.* 23:1626–1634.

Robinson, D. A., and Kukla, G. (1985), Maximum surface albedo of seasonally snow-covered lands in the Northern Hemisphere. *J. Clim. Appl. Meteorol.* 24:402–411.

Running, S. W., Justice, C. O., Salomonson, V. V., et al. (1994), Terrestrial remote sensing science and algorithms planned for EOS/MODIS. *Int. J. Remote Sens.* 15(17):3587–3620.

Salomonson, V. V., Toll, D. L., and Lawrence, W. T. (1992), The moderate resolution imaging spectrometer (MODIS) and observations of the land surface. In *Proceedings of the IGARSS '92 Symposium*, 26–29 May, pp. 549–551.

Scharfen, G. R., Hall, D. K., and Riggs, G. A. (1997), MODIS snow and ice products from the NSIDC DAAC. In *Proceedings of SPIE*, 27 July–1 August, San Diego, CA, pp. 143–147.

Townshend, J. R. G., Tucker, C. J., and Goward, S. N. (1993), Global vegetation mapping. In *Atlas of Satellite Observations Related to Global Change* (R. J. Gurney, J. L. Foster, and C. L. Parkinson, Eds.), Cambridge University Press, London, pp. 301–311.